Suffusion-induced evolution of microstructure and mechanical properties of internally unstable soils using CFD-DEM

Zheng Hu[1], Zhongxuan Yang[2], Yida Zhang[3]

[1] Sun Yat-sen University, China
[2] Zhejiang University, China
[3] University of Colorado Boulder, USA

2 Feb, 2021

Outline

- Introduction
- Methodology & Benchmarks
- Simulation procedures
- Simulation results
- Conclusions & Outlooks

Introduction

◻ Dam Failure and Accidents

❖ Interaction between soils and water

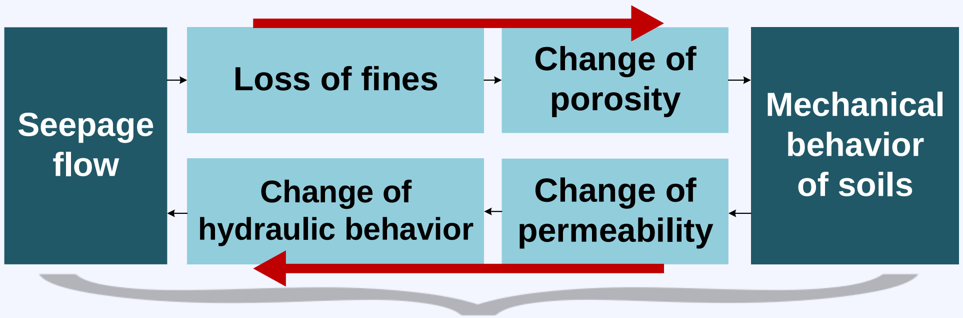

Internal Erosion Consequences on Dams
Slope failure, Settlement, Sinkhole

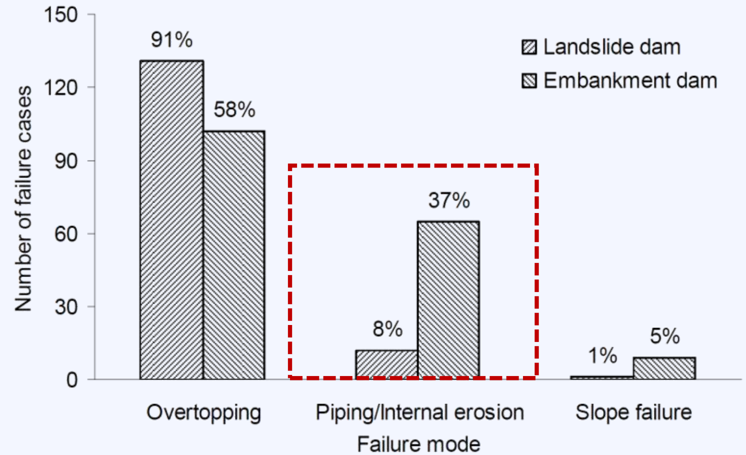

* Data from Peng & Zhang (2012)
* **144** landslide dams and **176** man-made earth and rockfill dams

❖ Internal erosion

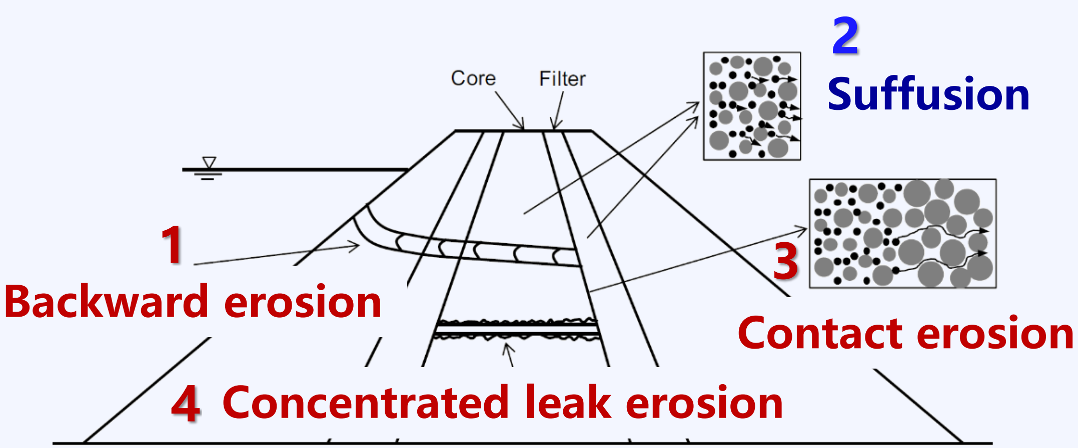

(Fell and Fry, 2007)

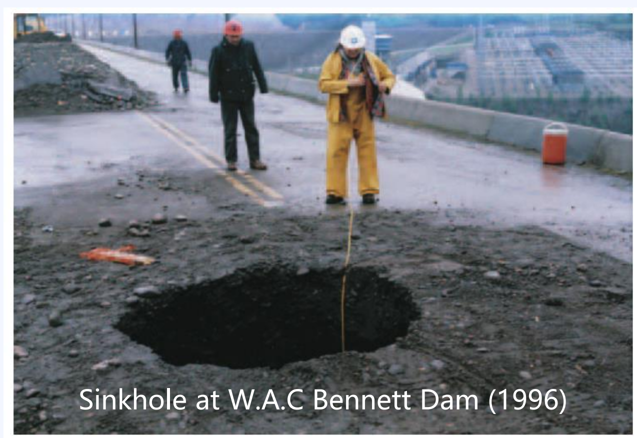

Sinkhole at W.A.C Bennett Dam (1996)

Introduction

Internal Erosion
Multiply variables: geometry, mechanical, and hydraulic conditions

Numerical simulations

Manually change PSD → **Pure DEM**
e.g. PFC, YADE

Without considering the nonuniformity of soil specimen

Laboratory experiments

Lab and site experiments
e.g. piping, suffusion ← Limitation of monitor technique

Without considering the micro evolution of erosion

Lack of a reliable theoretical method for internal erosion
Initiation, evolution and failure of soils during internal erosion

CFD-DEM coupling method
Applied in Geotechnics

Reproducing suffusion process and mechanical responses

Evolution of
Force chain, clogging effects, local piping, solid/void space, contact network

Methodology & Benchmarks

Soil particles ⟷ Seepage field

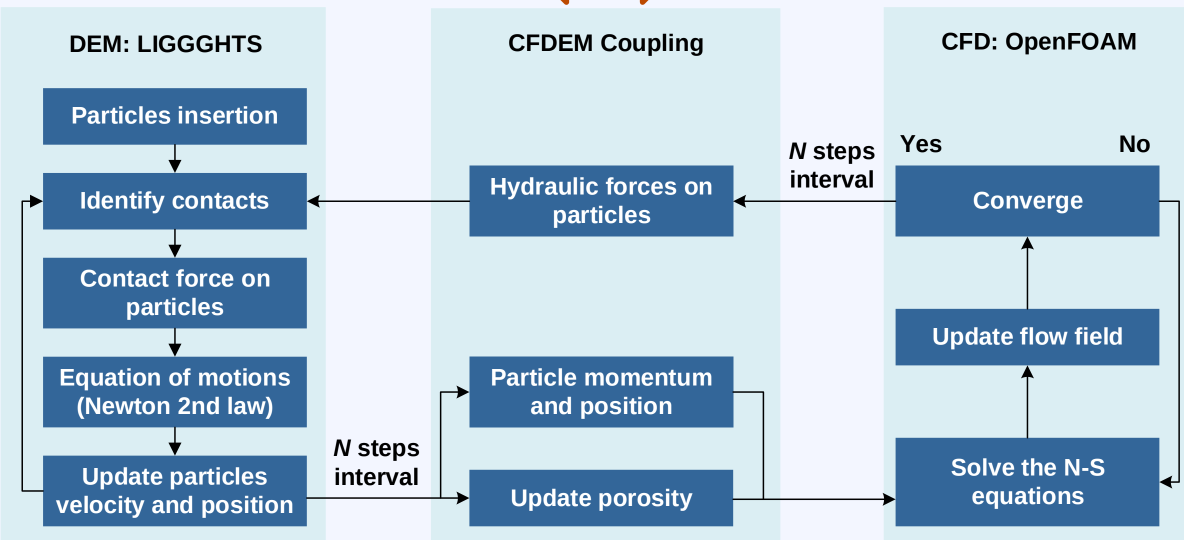

Ligghts Governing equation

$$m_i \frac{d\mathbf{U}_i^p}{dt} = \sum_c \mathbf{F}_{ij}^c + \mathbf{F}_i^g + \mathbf{F}_{pi}^f$$

$$I_i \frac{d\boldsymbol{\omega}_i}{dt} = \sum_c \mathbf{M}_{ij}^c$$

$$\mathbf{M}_r = -\frac{\boldsymbol{\omega}_{rel}}{|\boldsymbol{\omega}_{rel}|} \mu_r \mathbf{F}_n R_r$$

rolling resistance

+

OpenFOAM N-S equation

$$\frac{\partial(n\rho_f \mathbf{U}^f)}{\partial t} + \nabla\cdot(n\rho_f \mathbf{U}^f\mathbf{U}^f) - n\nabla\cdot(\mu_f \nabla \mathbf{U}^f) = -\nabla p - \mathbf{f}_f^p + n\rho_f \mathbf{g}$$

+

CFDEM Interaction force

$$\mathbf{F}_p^f = \mathbf{F}_d + \mathbf{F}_v + \mathbf{F}_g$$

$$\mathbf{F}_d = \frac{1}{2} C_d \rho_f \pi r_p^2 |\mathbf{U}_f - \mathbf{U}_p| (\mathbf{U}_f - \mathbf{U}_p) n^{2-\chi}$$

$$\mathbf{F}_g = -V_s \nabla p$$

$$\mathbf{F}_v = -V_s \nabla\cdot\boldsymbol{\tau}$$

Divided void fraction method

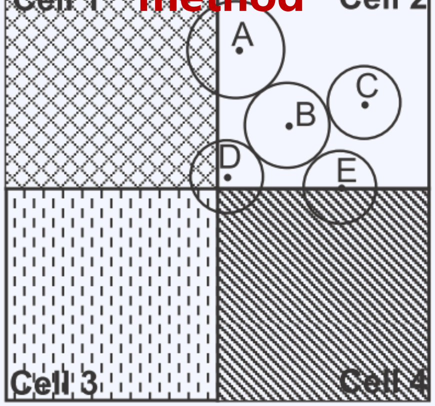

$$\alpha = v_{ij}^p / v_i^p \quad \alpha \in [0,1]$$

Consolidation process

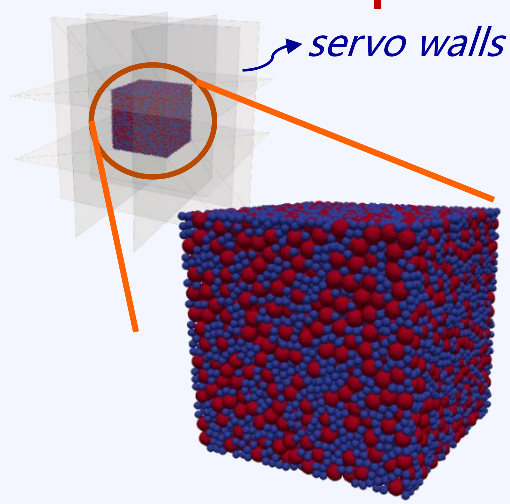

Methodology & Benchmarks

☐ Sedimentation of a sphere

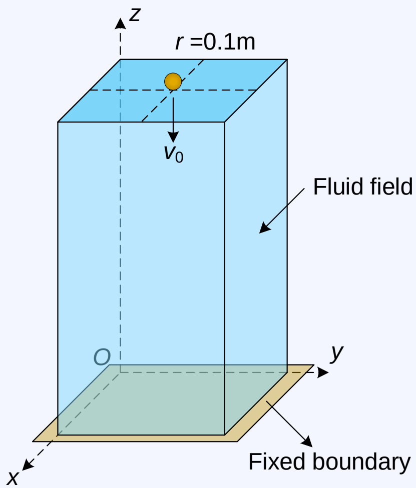

$$\frac{4}{3}\pi r_{\mathrm{p}}^{3}\rho_{\mathrm{s}}\frac{\partial \mathbf{U}_{\mathrm{r}}}{\partial t}=\frac{4}{3}\pi r_{\mathrm{p}}^{3}\left(\rho_{\mathrm{s}}-\rho_{\mathrm{f}}\right)\mathbf{g}-\frac{1}{2}\pi r_{\mathrm{p}}^{2}\rho_{\mathrm{f}}C_{\mathrm{d}}\mathbf{U}_{\mathrm{r}}^{2}$$

(Zhao *et al.*, 2014 & 2017)

☐ 1D Consolidation

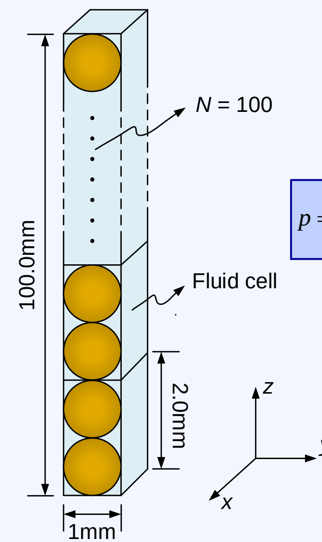

$$p=\sum_{m=1}^{\infty}\frac{2p_0}{m\pi}(1-\cos m\pi)\sin\frac{m\pi z}{2H}\exp\left(-\frac{m^2\pi^2T_{\mathrm{v}}}{4}\right)$$

(Budhu, 2011)

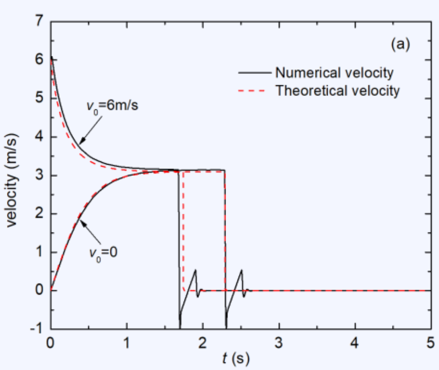

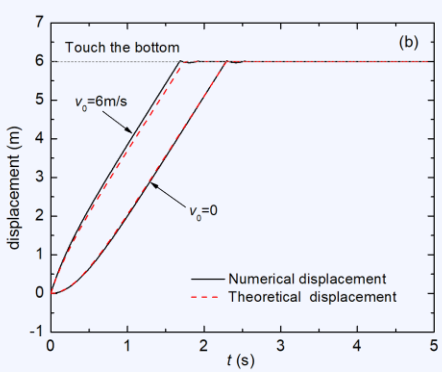

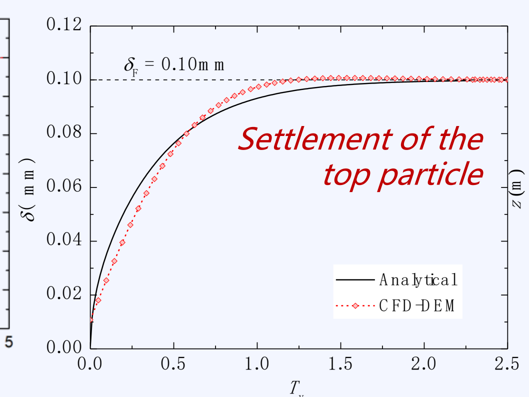

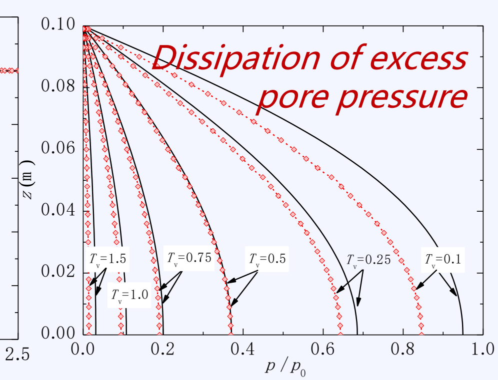

Simulation procedures

□ Sample preparation and suffusion

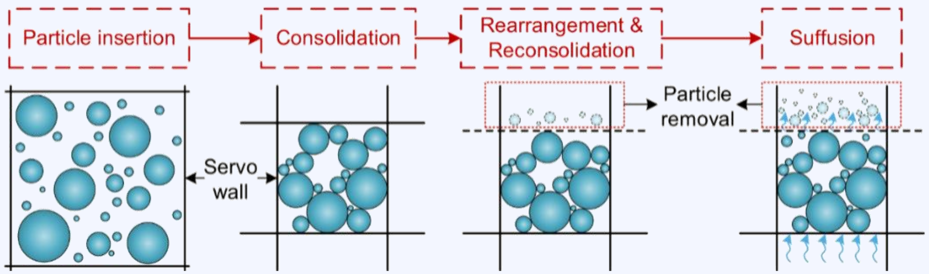

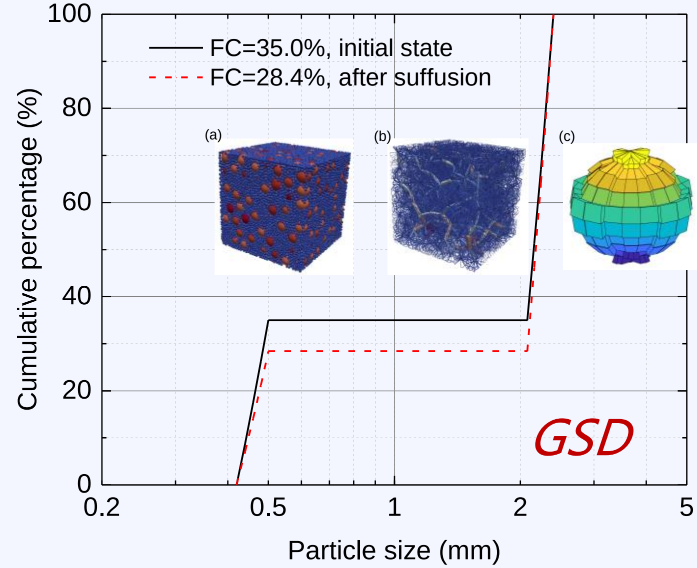

□ Model parameters

Computation modules	Parameter types (units)	Values
Solid phase (DEM) 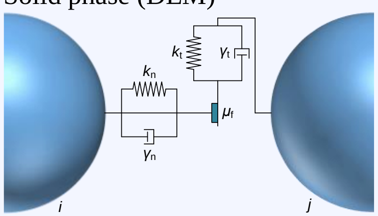	Particle number	26,267
	Particle diameter (mm)	0.42 ~ 2.40
	Particle density (kg/m^3)	2.65×10^3
	Young's modulus (GPa)	70
	Poisson's ratio	0.3
	Coefficient of friction	0.5
	Coefficient of restitution	0.2
	Coefficient of rolling friction	0.1
Fluid phase (CFD)	Fluid density (kg/m^3)	1.00×10^3
	Dynamic viscosity (Pa·s)	1.00×10^{-3}
	Size of fluid cells (mm)	3.2
Soil-water interaction (CFD-DEM)	timestep of DEM (s)	2.00×10^{-7}
	timestep of CFD (s)	2.00×10^{-5}
	Coupling interval (s)	2.00×10^{-5}
	Simulation real time (s)	15

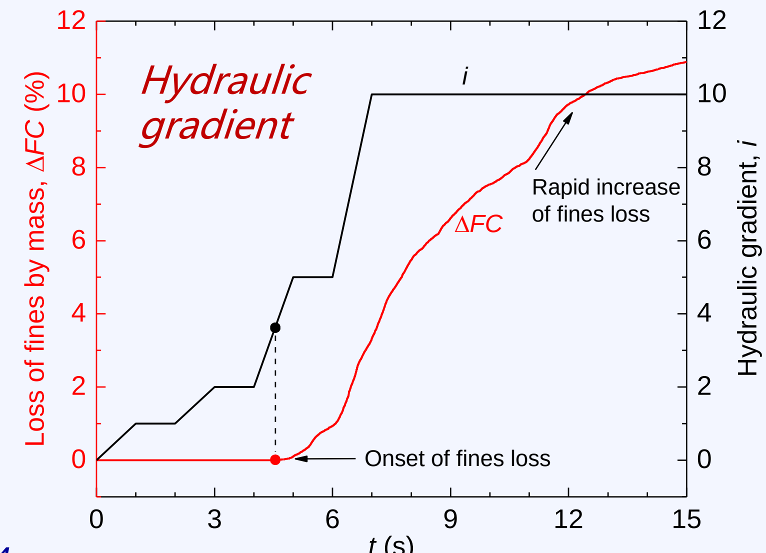

Hu, Z., Zhang, Y., & Yang, Z. (2019). Acta Geotechnica, 14(3), 795-814.

Simulation procedures

□ Procedures of simulations using different methods

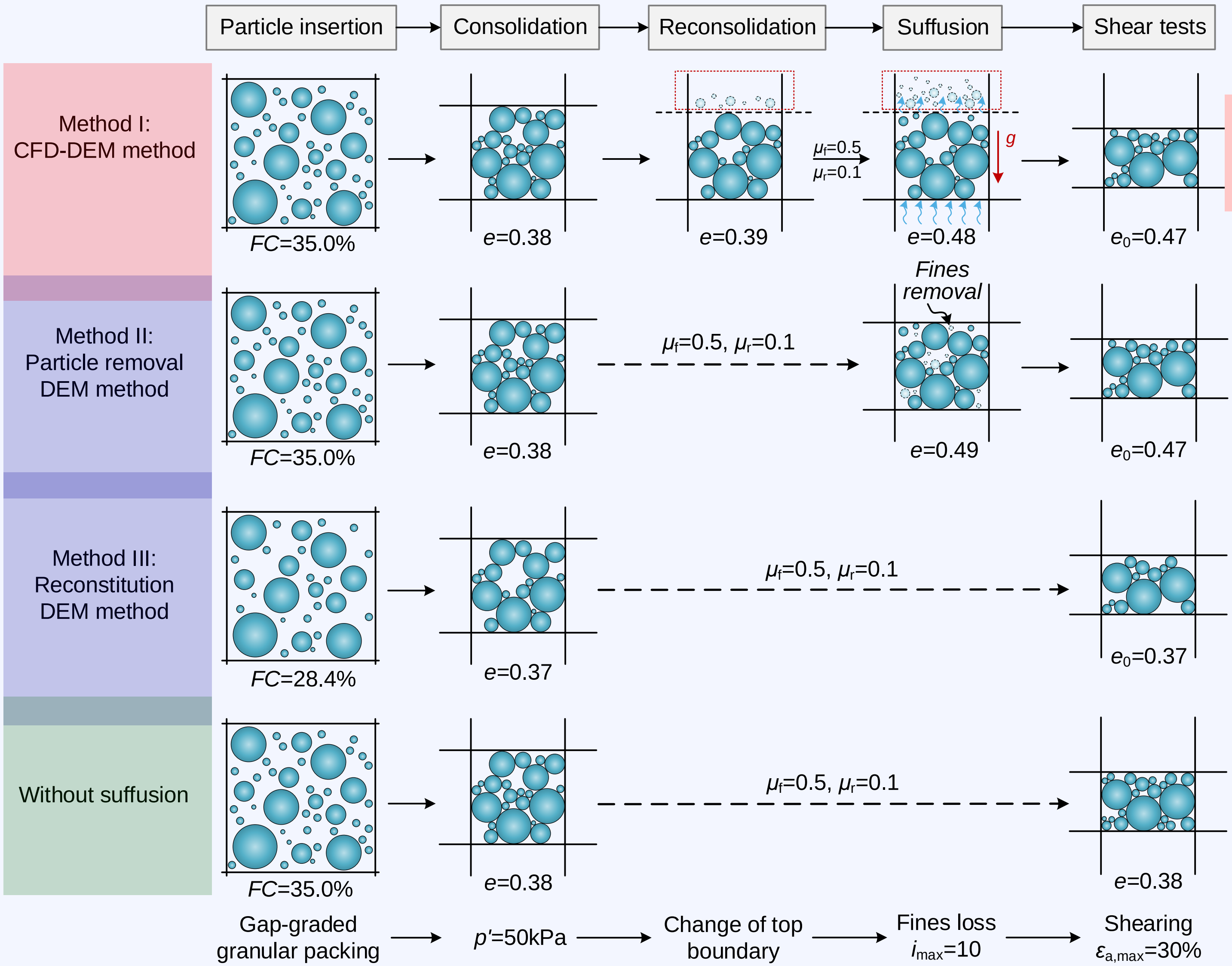

- Geometric conditions
- Stress conditions
- Hydraulic conditions

Results from suffusion stage

□ Particle assembly and flow field — End of suffusion

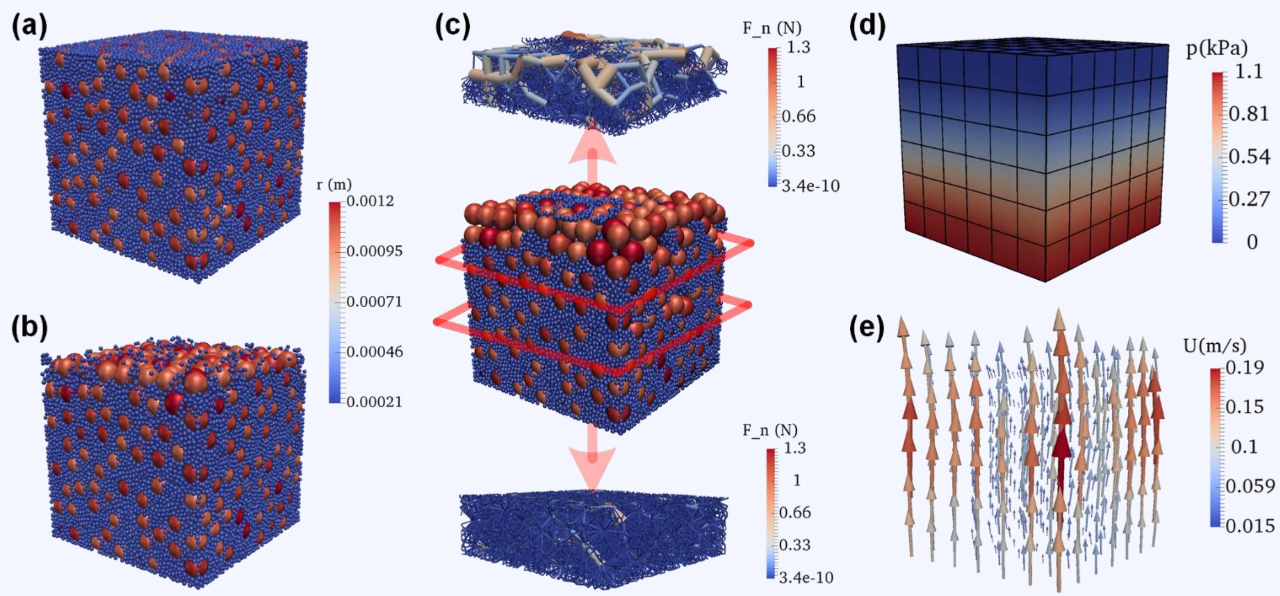

□ Loss of fines and volumetric deformation

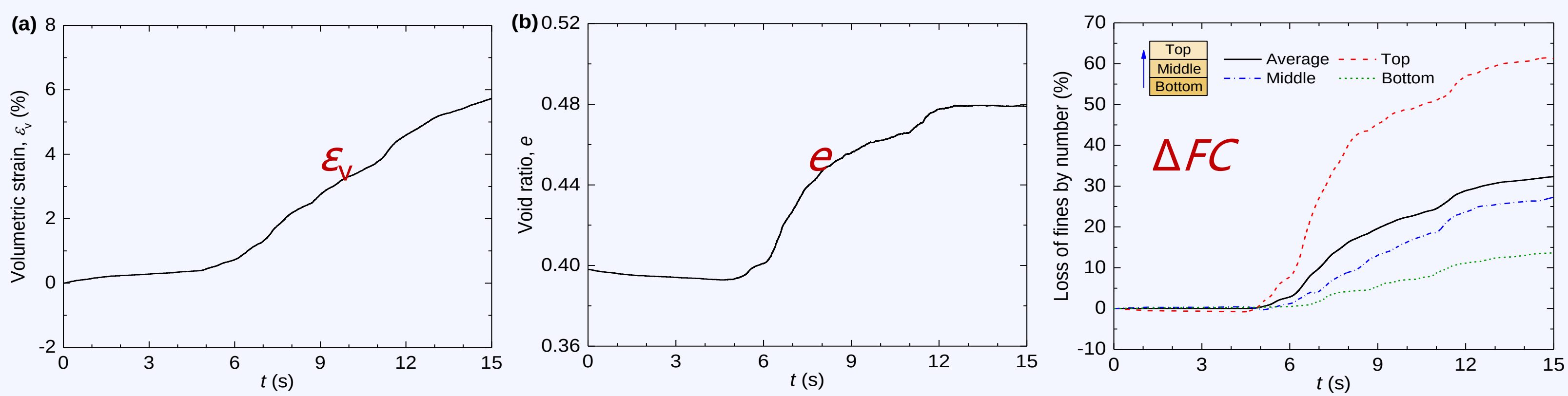

Results from suffusion stage

□ Evolution of void ratio and active fine particles

- ✓ Active fine particles： Connectivity ≥ 2
- ✓ Intergranular void ratio e_c： Only coarse particles
- ✓ Equivalent intergranular void ratio e_e： Only active particles

$$e_{\mathrm{c}} = \frac{e + f_{\mathrm{f}}}{1 - f_{\mathrm{f}}} \qquad e_{\mathrm{e}} = \frac{e + \left(1 - f_{\mathrm{a}}\right)}{f_{\mathrm{a}}}$$

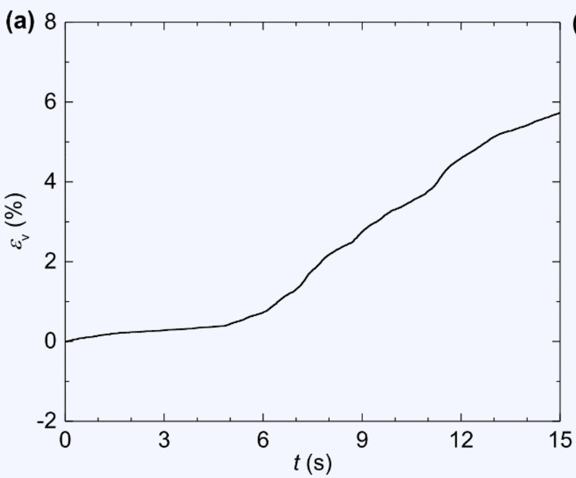

Volumetric strain

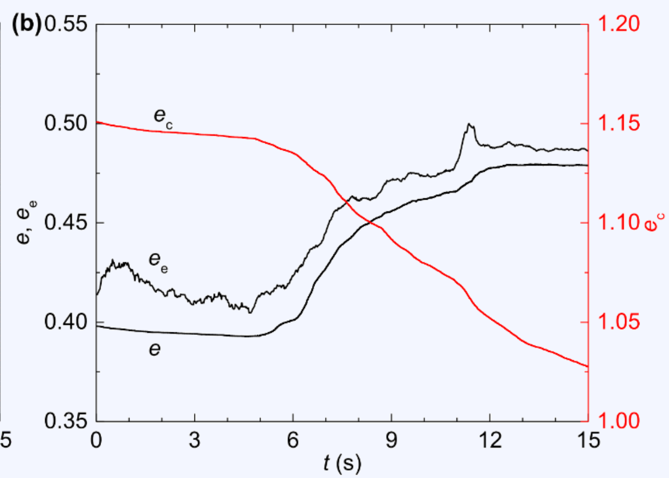

Void ratio

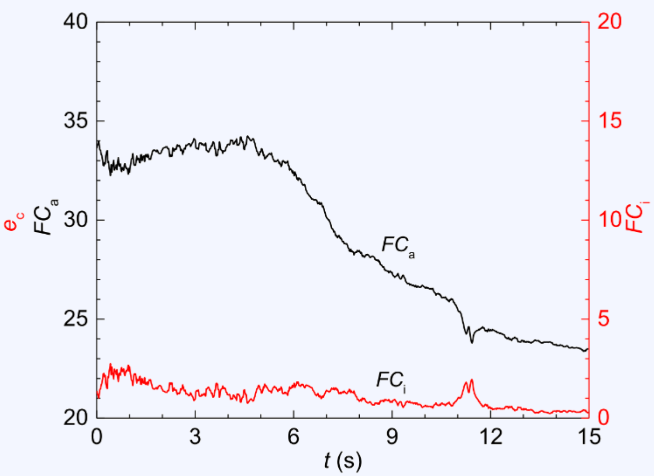

Active fine particles

Results from suffusion stage

◻ Acceleration of fines due to seepage

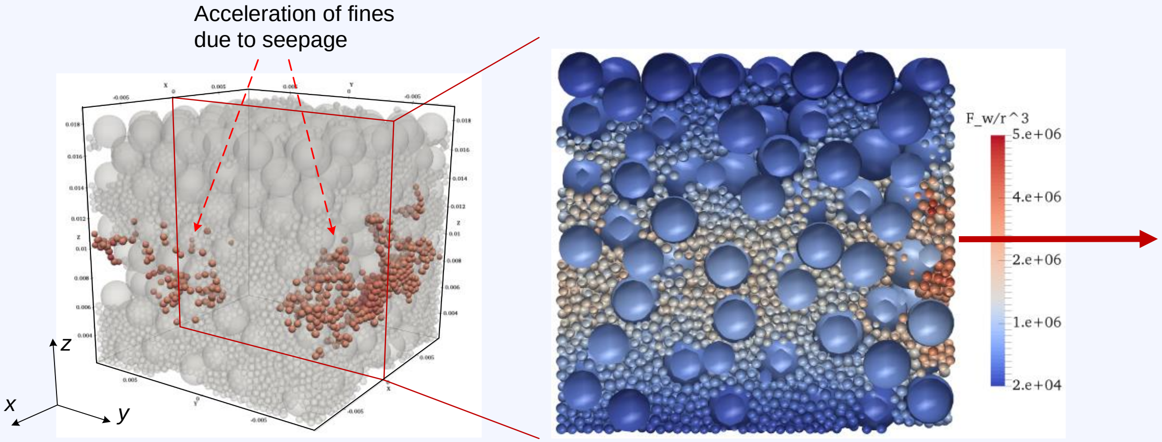

Preferential flow paths near the lateral boundary

◻ Evolution of local piping erosion

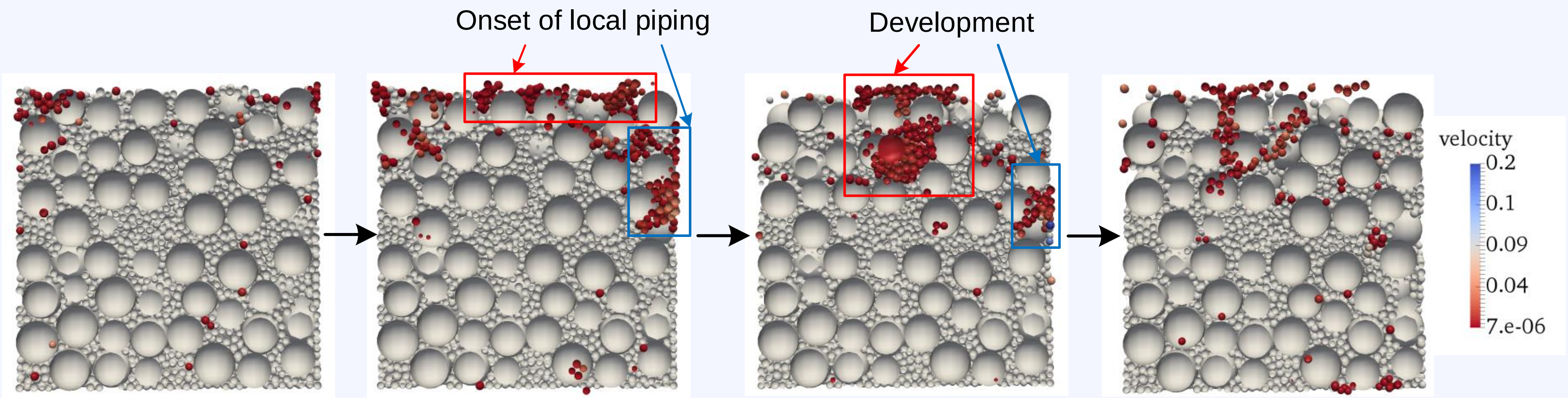

I: *t*=6s
II: *t*=6.5s
III: *t*=7s
IV: *t*=7.5s

Results from suffusion stage

☐ Sudden blowout of fine clusters *t* = 11s

- ✓ Rapid loss of active fines; the sample deforms significantly;
- ✓ Local strong force chain is broken and a pseudo stable skeleton is reformed.

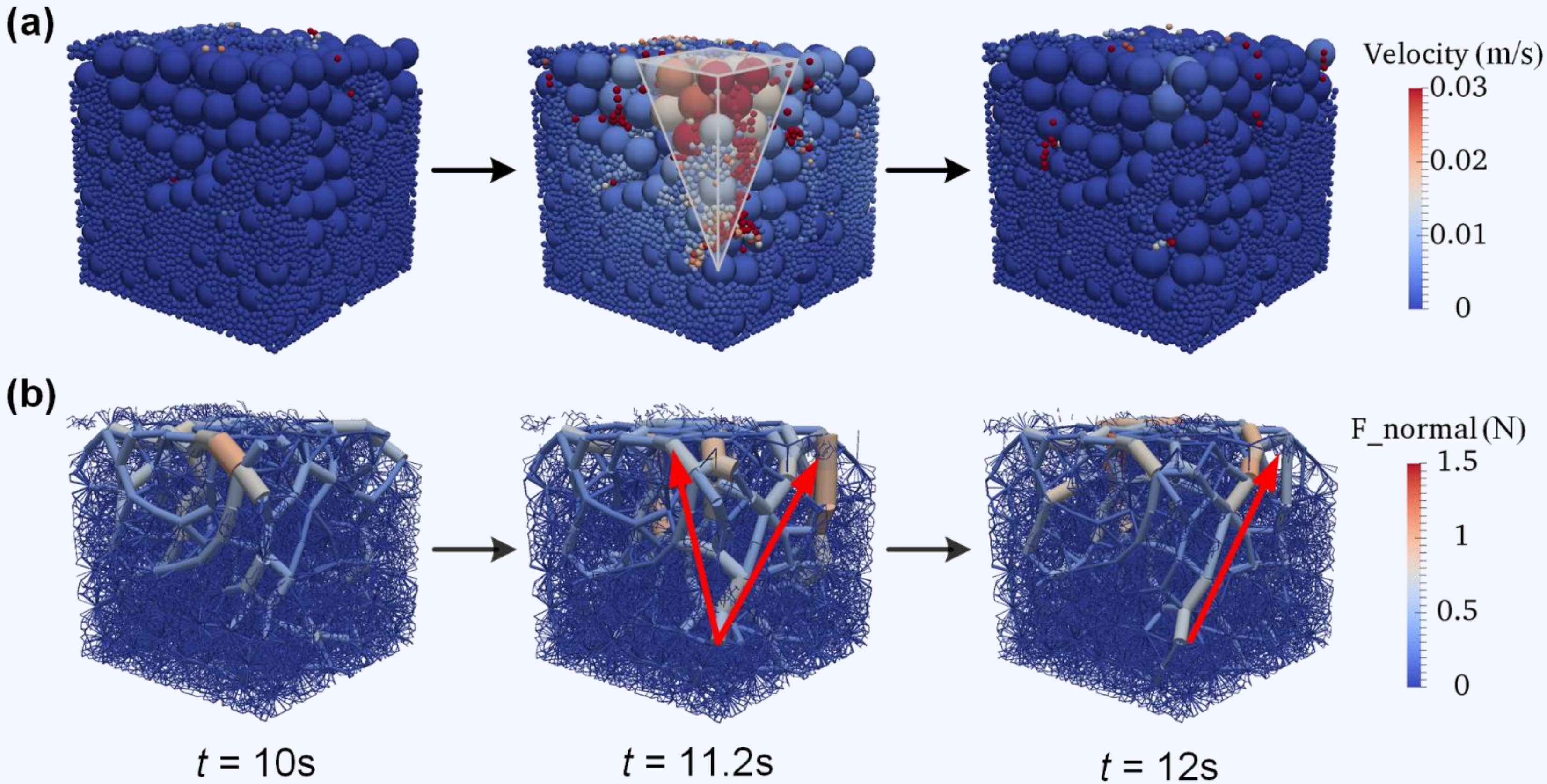

Results from shear stage

□ Shear behavior before and after suffusion

Method I **CFD-DEM method;**
Method II **DEM particle removal method: strain-hardening;**
Method III **DEM reconstitution method: strain-softenning.**

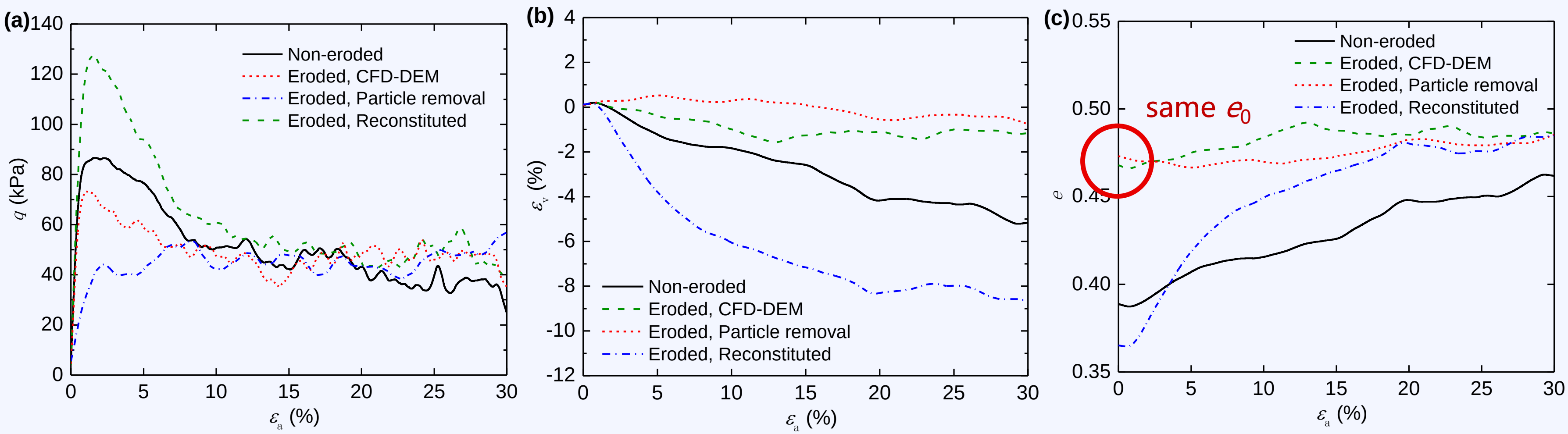

The same GSD and e_0 of samples from CFD-DEM and particle removal method, **different stress-strain responses?**

Results from shear stage

◻ Evolution of (equivalent) intergranular void ratio

- ✓ CFD-DEM sample: more fines participate in the force chain network;
- ✓ The enhanced initial stiffness and peak shear strength of the eroded soil.

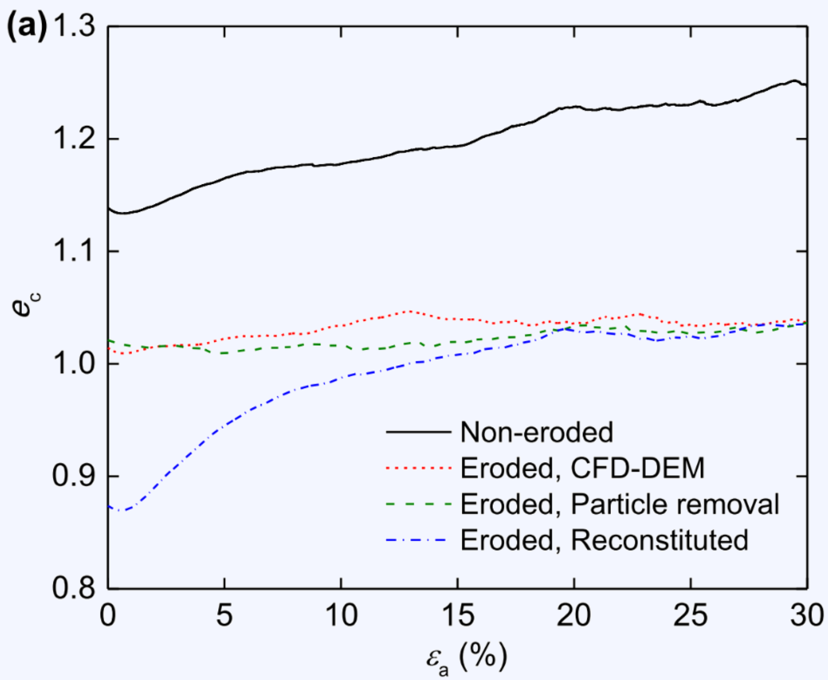

Intergranular void ratio

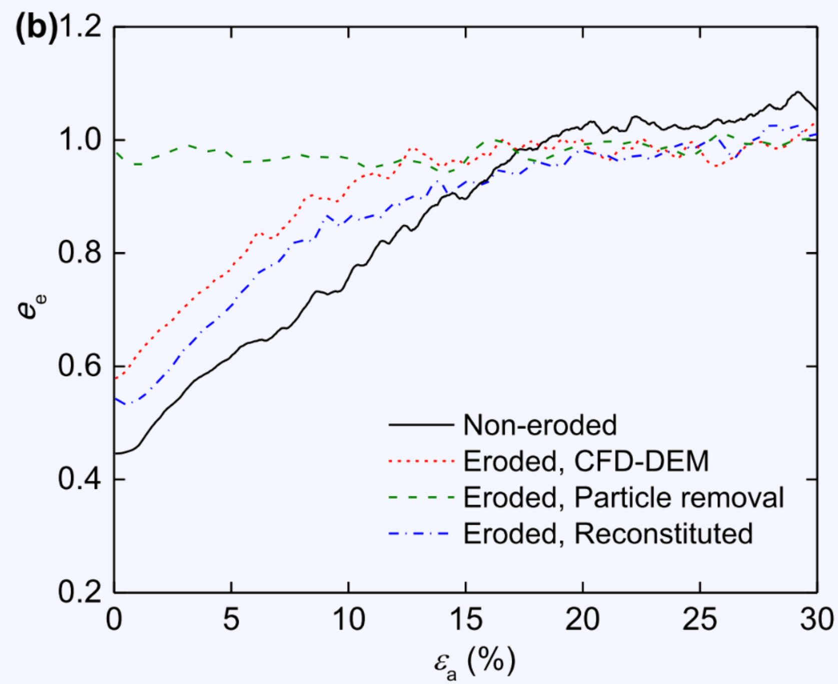

Equivalent intergranular void ratio

Microstructural inspections

□ Evolution of coordination number

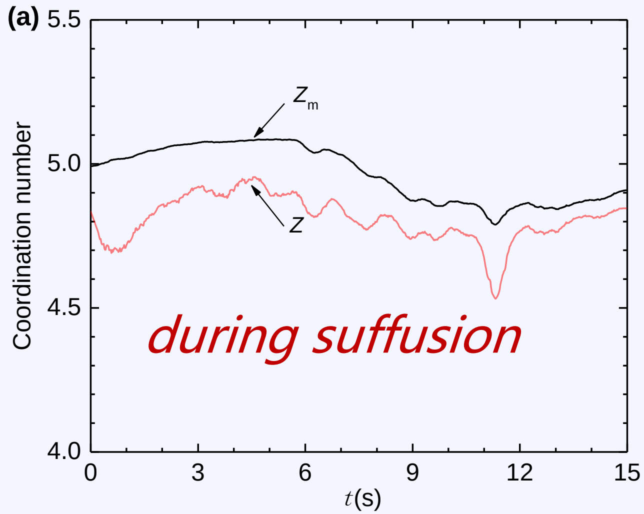

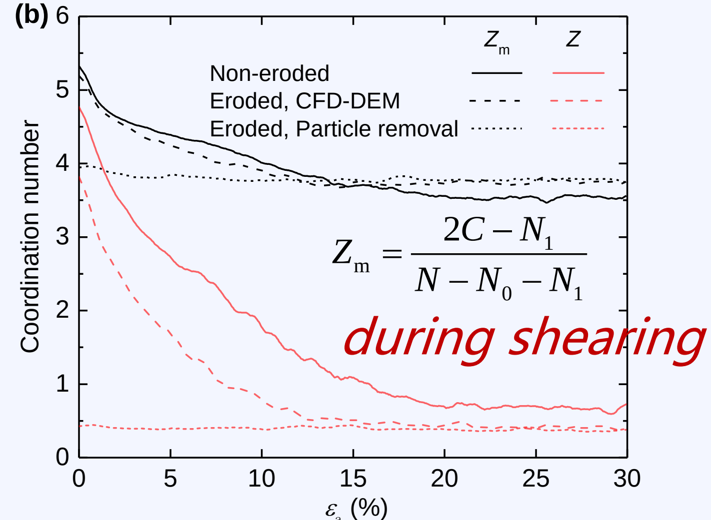

□ Distribution of particle connectivity

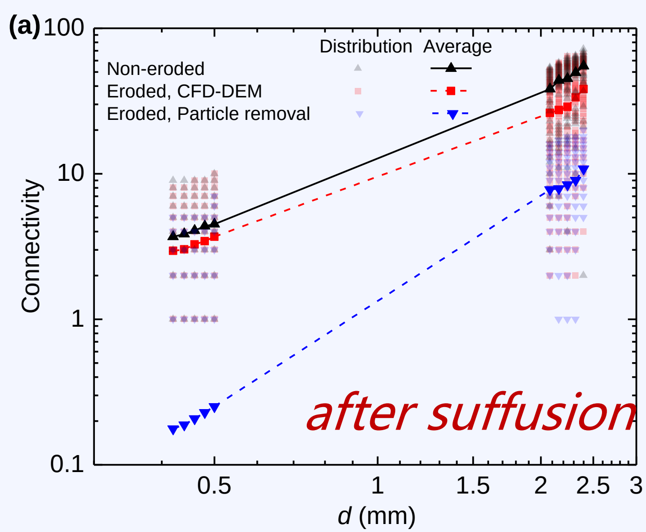

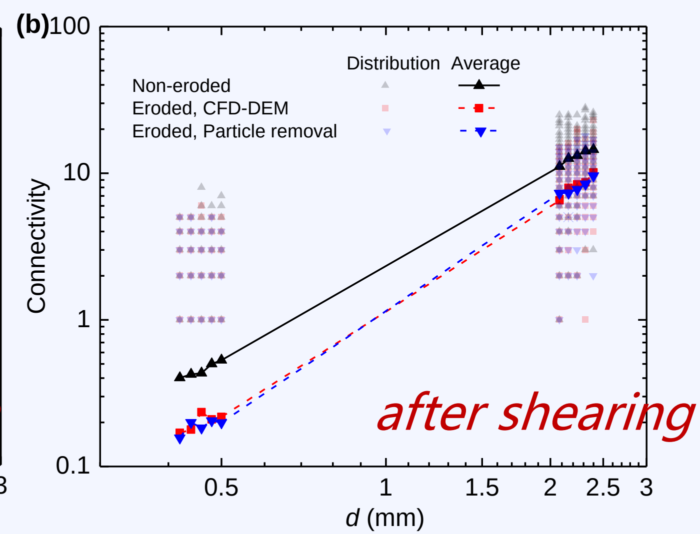

Microstructural inspections

□ Void characteristic of the sample

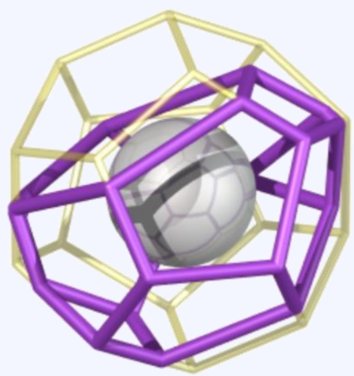

Voronoi tessellation

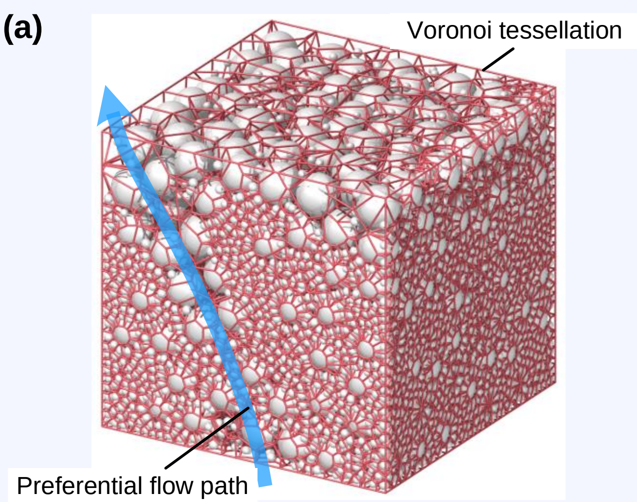

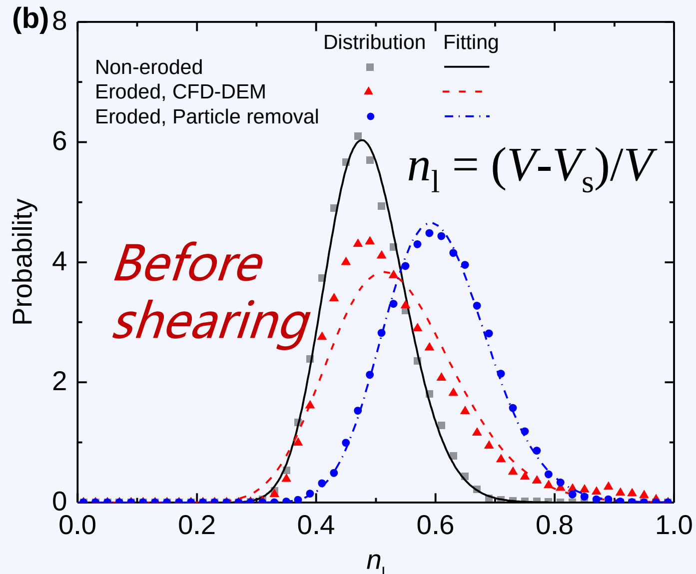

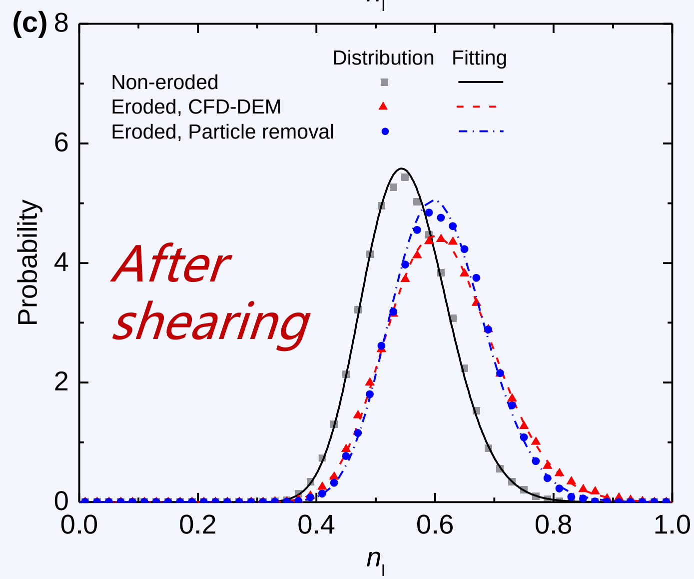

void fraction distribution

+

Void ratio, e

Microstructural inspections

◻ Force chain and contact norms Before shear tests

Non-eroded | Eroded, CFD-DEM | Eroded, Particle removal

Contact force chain

Contact norms

Contact normal force

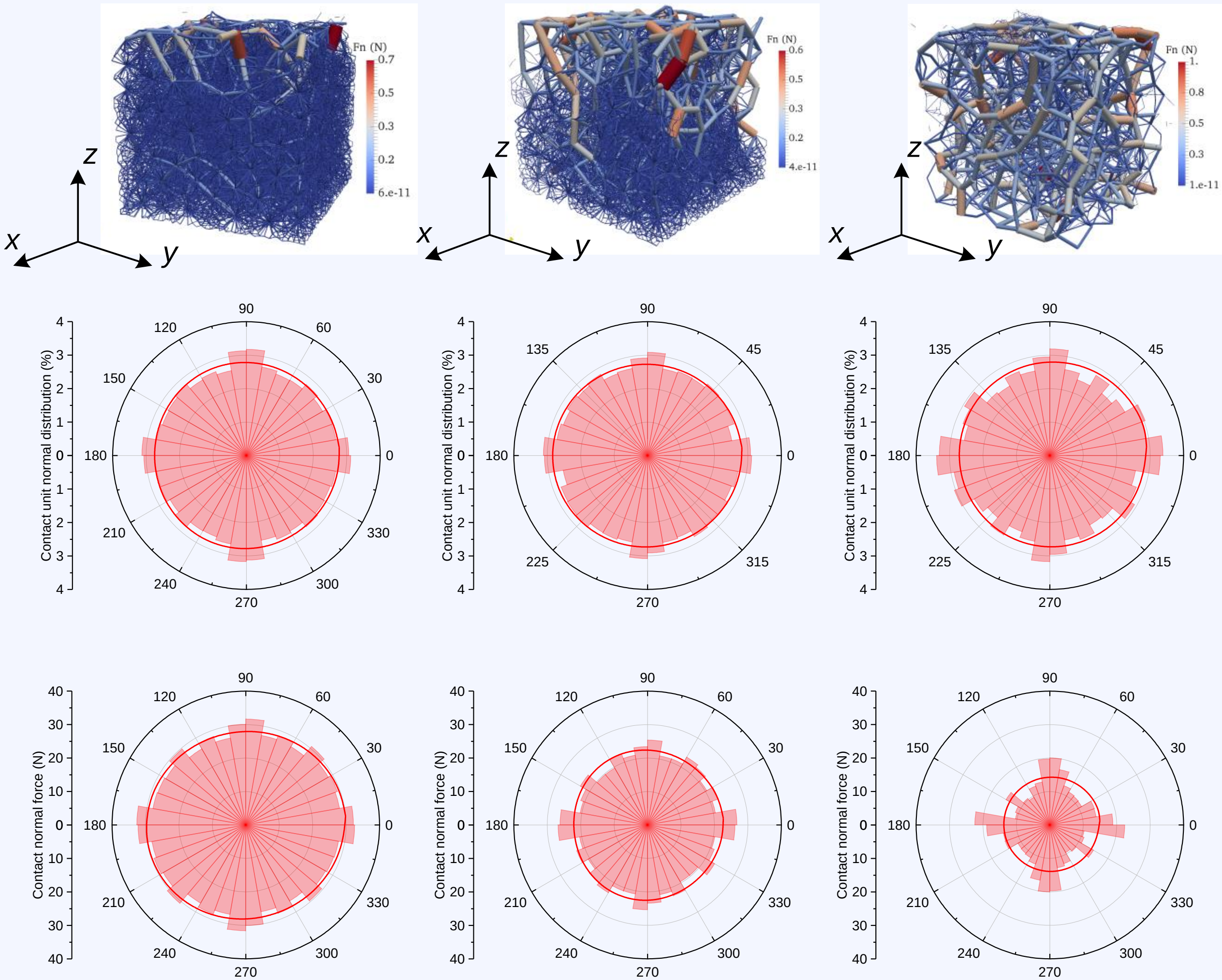

Microstructural inspections

◻ Force chain and contact norms After shear tests

Non-eroded | Eroded, CFD-DEM | Eroded, Particle removal

Contact force chain

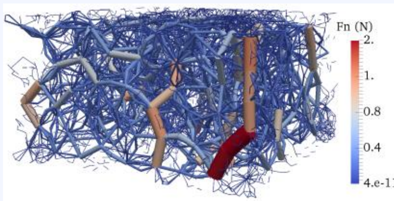

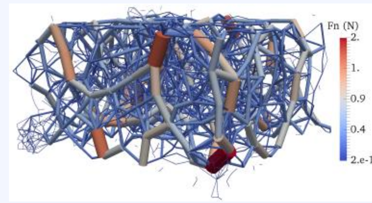

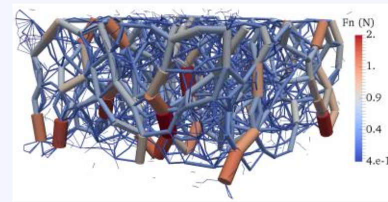

Contact norms

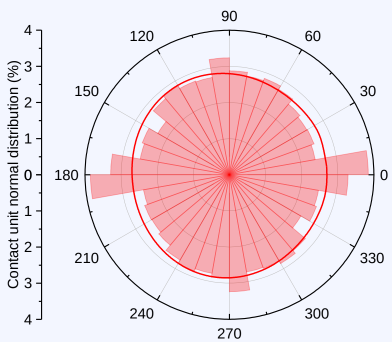

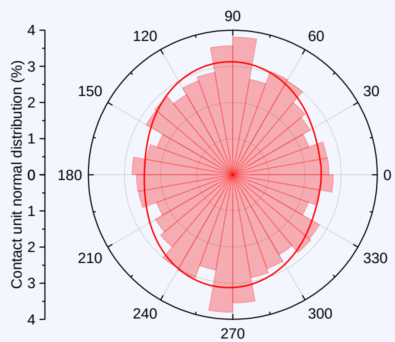

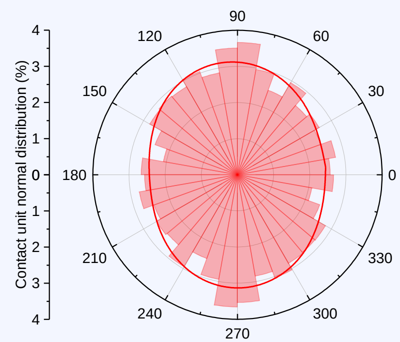

Contact normal force

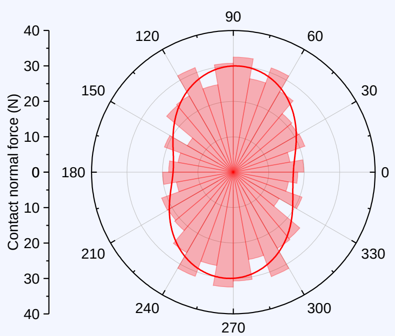

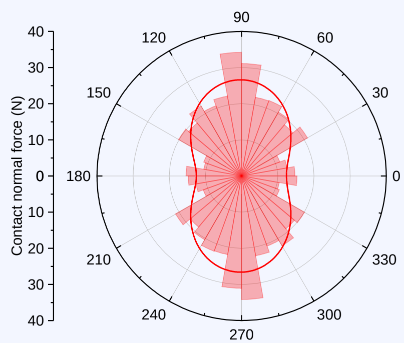

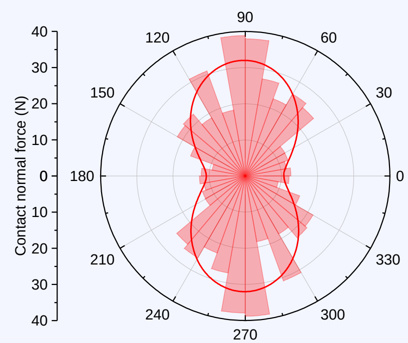

Circular

↓

Elliptical Peanut-shape

Conclusions

- **Reproduction of suffusion process:** The entire suffusion process can be reasonably captured by the present coupling method.

- **Non-uniform distribution of particles:** The erosion rate varies, leading to non-uniformity, preferential flow paths and intermittent local piping.

- **Mechanical behavior of eroded specimen:** Not only affected by GSD, but also highly depends on its void distribution and fabric structure.

- **Microstructural inspections:** The different mechanical response of the CFD-DEM eroded specimen and the others are caused by the large number of active fines participated in the force transmission.

- **Critical state and anisotropy:** All eroded samples (which have the same GSD) approached to the same average and mechanical coordination number, connectivity, void fraction distribution and contact statistics.

Thanks for your attention!

E-mail: huzheng6@mail.sysu.edu.cn